



MiRNA-137-mediated modulation of mitochondrial dynamics regulates human neural stem cell fate

Asha S. Channakkar¹ | Tanya Singh^{1,2} | Bijay Pattnaik³ | Karnika Gupta¹ | Pankaj Seth¹  | Yogita K. Adlakha¹ 

¹Molecular and Cellular Neuroscience, National Brain Research Centre, Manesar, India

²Neuroscience and Mental Health Research Institute, Cardiff University, Cardiff, United Kingdom

³Centre of Excellence in Asthma & Lung Disease, CSIR-Institute of Genomics and Integrative Biology, Delhi, India

Correspondence

Yogita K. Adlakha, PhD, Molecular and Cellular Neuroscience, National Brain Research Centre, Manesar-122052, India.
Email: yogita@nbrc.ac.in

Funding information

Department of Science and Technology, Ministry of Science and Technology, India; National Brain Research Centre

Abstract

The role of miRNAs in determining human neural stem cell (NSC) fate remains elusive despite their high expression in the developing nervous system. In this study, we investigate the role of miR-137, a brain-enriched miRNA, in determining the fate of human induced pluripotent stem cells-derived NSCs (hiNSCs). We show that ectopic expression of miR-137 in hiNSCs reduces proliferation and accelerates neuronal differentiation and migration. TargetScan and MicroT-CDS predict myocyte enhancer factor-2A (MEF2A), a transcription factor that regulates peroxisome proliferator-activated receptor-gamma coactivator (PGC1 α) transcription, as a target of miR-137. Using a reporter assay, we validate MEF2A as a downstream target of miR-137. Our results indicate that reduced levels of MEF2A reduce the transcription of PGC1 α , which in turn impacts mitochondrial dynamics. Notably, miR-137 accelerates mitochondrial biogenesis in a PGC1 α independent manner by upregulating nuclear factor erythroid 2 (NFE2)-related factor 2 (NRF2) and transcription factor A of mitochondria (TFAM). In addition, miR-137 modulates mitochondrial dynamics by inducing mitochondrial fusion and fission events, resulting in increased mitochondrial content and activation of oxidative phosphorylation (OXPHOS) and oxygen consumption rate. Pluripotency transcription factors OCT4 and SOX2 are known to have binding sites in the promoter region of miR-137 gene. Ectopic expression of miR-137 elevates the expression levels of OCT4 and SOX2 in hiNSCs which establishes a feed-forward self-regulatory loop between miR-137 and OCT4/SOX2. Our study provides novel molecular insights into NSC fate determination by miR-137.

KEYWORDS

fission, human induced pluripotent stem cells, miRNA, mitochondria dynamics, mitochondria fusion, mitochondrial biogenesis, neural stem cells, neurodevelopment

1 | INTRODUCTION

Neural development involves dynamic and adaptive processes that function in an extremely constrained and genetically orchestrated context. In addition to gene regulatory networks, post-transcriptional mechanisms play an evident role in neural development.^{1,2} Disruptions in the post-

Abbreviations: ETC, electron transport chain; hiNSCs, human induced neural stem cells; MEF2A, myocyte-specific enhancer factor 2A; NRF2, nuclear factor erythroid 2 (NFE2)-related factor 2; OCR, oxygen consumption rate; OXPHOS, oxidative phosphorylation; PGC1 α , peroxisome proliferator-activated receptor-gamma coactivator.

Asha S. Channakkar and Yogita K. Adlakha contributed equally to this work.

This is an open access article under the terms of the Creative Commons Attribution-NonCommercial License, which permits use, distribution and reproduction in any medium, provided the original work is properly cited and is not used for commercial purposes.

©2020 The Authors. STEM CELLS published by Wiley Periodicals, Inc. on behalf of AlphaMed Press 2020

transcriptional mechanisms during neural development lead to aberrant brain growth that result in neurodevelopmental disorders.^{3,4} To understand the pathogenesis of neurodevelopmental disorders, post-transcriptional regulatory mechanisms which operate during neural stem cell (NSC) fate determination need to be investigated.

MicroRNAs are short noncoding RNAs of 20-25 nucleotides that constitute a part of the post-transcriptional regulation and fine-tune gene expression.⁵ They play important roles in several physiological processes including development, proliferation, differentiation, and apoptosis.⁶⁻⁸ Neural development implicates several miRNAs which refine the gene expression at various stages including the initial specification of neuronal cell types, formation, maturation, and plasticity of synapse.⁹ In addition, the brain expresses specific miRNAs which aid in attaining specific fate during NSC fate determination.

MiR-137 is a brain-enriched miRNA which harbors binding sites of key pluripotency transcription factors including OCT4, SOX2, and NANOG in the promoter of its gene.¹⁰ Single nucleotide polymorphism and chromosomal microdeletion in miR-137 host gene associate miR-137 to neurological diseases.^{11,12} Dysregulation of miR-137 has been implicated in several neurodevelopmental disorders and cancers.¹³⁻²¹ Studies based on mouse model indicate that miR-137 promotes neuronal differentiation, while inhibits cell proliferation.^{18,22-24} However, whether and how miR-137 regulates human NSCs fate has not been investigated.

Increasing evidence suggests that neural development involves a metabolic shift during differentiation of NSCs to neurons, whereby prevalent glycolytic metabolism of NSCs shift to OXPHOS to meet high metabolic requirements of neurons.²⁵⁻²⁷ This process is associated with an increase in mitochondrial biogenesis, mitochondria fusion, fission, and changes in mitochondrial morphology.²⁷⁻²⁹ Mitochondria dynamics is now emerging as a crucial upstream regulator of NSC fate decisions.³⁰ Despite this, the detailed molecular mechanism of alteration of mitochondrial dynamics during NSCs fate decision remains unknown.

We propose that miR-137 might modulate human-induced NSCs (hiNSCs) fate determination by altering mitochondrial dynamics. Here, our study provides evidence that miR-137 inhibits hiNSC proliferation, while enhances neuronal differentiation and migration. We demonstrate that miR-137 downregulates MEF2A which is an upstream regulator of PGC1 α . We show that miR-137 modulates mitochondrial dynamics by accelerating mitochondrial biogenesis, fusion and fission, and OXPHOS. In addition, miR-137 increases the expression of pluripotency transcription factors, OCT4 and SOX2, which in turn bind to the promoter of miR-137. Our observations indicate that miR-137 forms a regulatory loop with OCT4/SOX2 during hiNSC fate determination. Thus, our study reveals a crucial role of miR-137 in hiNSC fate determination and possible underlying molecular mechanism.

2 | MATERIALS AND METHODS

2.1 | Derivation of induced iPSCs

Peripheral blood mononuclear cells (PBMCs) were harvested from healthy subjects after obtaining their informed consent. The blood

Significance statement

The derivation of human neural stem cells (hNSCs) from human iPSCs that faithfully display immunoreactivity toward NSC markers and serve as a model to study neurological diseases is described. Using this model, the role of a brain-enriched small noncoding RNA, miR-137, is shown. It enhances neuronal differentiation by inducing mitochondrial biogenesis, fusion, fission, and OXPHOS. The decrease in NSCs with age likely leads to compromised regenerative capacity of the brain. This study proposes that NSC differentiation induced by miR-137 may facilitate the design of treatments for aging-associated neurodegenerative diseases.

cells were processed according to the protocol approved by the Institutional Human Ethics and Stem Cell Research Committee of National Brain Research Centre, India (IRB00007523). CD34+ mononuclear cells were enriched from PBMC population using magnetic activated cell sorting kit (Miltenyi Biotec, Singapore). 1×10^5 CD34+ cells were transduced with integration-free Cytotune Sendai Reprogramming kit to derive induced pluripotent stem cells (iPSCs) as described previously.³¹ The iPSCs were maintained on Geltrex (Gibco, Waltham, MA)-coated plates using a chemically defined Essential 8 medium (Gibco) with medium changed every day. These cells were passaged every 3-4 days at ~70%-80% confluency using EDTA.³² Colonies were maintained in a pluripotent state and any differentiated cells around colonies were marked and removed mechanically before passaging. These cell lines were verified for iPSC markers by immunocytochemistry, qRT-PCR, and Western blot.

2.2 | Derivation and culture of hiNSCs

The iPSCs were induced to differentiate toward neural ectodermal lineage to generate NSCs. As they were derived from human iPSCs, hence we named them hiNSCs. Briefly, iPSC colonies were seeded on Geltrex (Corning, NY)-coated six-well plate. After achieving 50% confluency, iPSC media was replaced with 1X StemPro NSC serum-free medium (Gibco) supplemented with 1X StemPro Neural Supplement, 20 ng/mL epidermal growth factor (EGF), 20 ng/mL basic fibroblast growth factor (bFGF), 2 mM Glutamax (Invitrogen, San Diego, CA) and 1X penicillin and streptomycin solution (Invitrogen). Cells were passaged at least seven times and characterized before performing experiments by assessing the expression of NSC markers SOX2 and Nestin by immunocytochemistry and qRT-PCR (Supplementary Figure S1). Almost 95% hiNSCs showed immunoreactivity toward SOX2 and Nestin. hiNSCs were further propagated as monolayer in 1X StemPro NSC serum-free medium (Gibco) at 37°C in a humidified atmosphere with the supply of 5% CO₂. For this study, hiNSCs were employed at passage number 6 to 10 for various assays.

2.3 | Neurosphere culture differentiation and migration assay

3×10^5 transfected hiNSCs were cultured as single cell suspension in 1X StemPro NSC serum-free medium (Gibco) (with EGF and FGF) and allowed to form neurospheres in a non-PDL-coated 25-cm² flask for 72 hours at 5% CO₂ and 37°C as described.³³ These neurospheres were seeded in 24-well plate containing PDL-coated coverslips and allowed to adhere. After attachment, the StemPro NSC serum-free medium was replaced with the neural differentiation medium (with PDGF and BDNF, as mentioned for neuronal differentiation) and maintained for 3 days. Three days post differentiation, neurospheres were fixed with 4% paraformaldehyde, blocked, and permeabilized using 5% BSA and 0.3% triton X-100. Cells were incubated with TUJ1 antibody (marker for newly formed neurons, 1:2000, Promega, G712A) as described in immunocytochemistry protocol. Images were captured using AxioImager.Z1 microscope (Carl Zeiss, Heidenheim, Germany). For migration assay, neurite length was traced from the periphery of the neurosphere using line tool in ImageJ software and three random measurements were obtained per neurosphere to ensure to cover the entire neurosphere for measurement. Length of the neurite corresponds to distance travelled by the neurite. For sprouting assay, the number of neurites per neurosphere were counted using the ImageJ software in three randomly chosen fields per neurosphere.^{34,35} For each experimental group, a minimum of five similar-sized neurospheres (diameter = $394 \pm 17.13 \mu\text{m}$) were imaged from three biological replicates.

2.4 | Differentiation of hiNSCs into neurons

1×10^5 hiNSCs were cultured on Poly D-lysine (PDL, Sigma-Aldrich, St. Louis, Missouri)-coated cover slips in 24-well plate and differentiated into neurons after replacing the StemPro NSC serum-free medium with neurobasal media (Invitrogen) supplemented with 1% N-2 supplement (Invitrogen), 1X Neural Survival Factor-1 (Lonza, Charles City, Iowa), 0.5% bovine serum albumin (Sigma-Aldrich), 2 mM glutamine (Sigma), 1X penicillin and streptomycin solution (Invitrogen), 0.05 mg/mL gentamycin (Sigma), 10 ng/mL brain derived neurotrophic factor (BDNF) (Peprotech, Rocky Hill, New Jersey), and 10 ng/mL platelet-derived growth factor (PDGF-AB) (Peprotech). The cells were maintained in differentiating media for at least 5 days. They were assessed for their immunoreactivity toward neuronal markers TUJ1 and DCX as described in our immunocytochemistry protocol.³⁵

2.5 | miRNA mimic/inhibitor transfection

5×10^5 hiNSCs were seeded in each well of six-well plate 1 day before transfection to achieve 70% to 80% confluency on the day of transfection. For mimic studies, 20 or 40 nM of miScript miR-137 mimic (Qiagen, Hilden, Germany) were used to transfect the cells using Lipofectamine RNAiMAX (Invitrogen). For anti-miR studies,

50 or 100 nM anti miScript miR-137 inhibitor (Qiagen) was used wherever indicated. Negative control (NC) siRNA and inhibitor control siRNA (Qiagen) were used as a NC for miRNA mimic and inhibitor, respectively. Results obtained by miR-137 mimic transfection were compared to NC and those obtained by anti-miR-137 transfection were compared to miR-137 mimic (40 nM) throughout manuscript.

2.6 | Plasmid constructs, luciferase reporter assays

This information is described in Supporting Information.

2.7 | Quantitative real-time PCR

RNA was extracted from transfected cells using the TRIzol (Invitrogen) and quantified using Nanodrop1000 Spectrophotometer (Applied Biosystems, Foster City, California). cDNA was prepared from RNA using High-Capacity cDNA Reverse Transcription Kit according to manufacturer's instructions (Applied Biosystems). qRT-PCR for genes was performed using cDNA (~25 ng/well) and Power SYBR Green PCR Master Mix (Applied Biosystems) on ViiA 7 Real-Time PCR System (Applied Biosystems). The relative fold change of an mRNA of interest was determined by normalization to RPL13A and HPRT1 mRNA through the $2^{-\Delta\Delta C_t}$ method.³⁶ Real-time detection of transcripts was performed in triplicate and repeated three times as described.³⁷ Single product peak in the melt curve analysis confirmed the specificity of primers used. The cycling conditions used for qPCR were 95°C for 10 minutes (1 cycle), followed by 40 cycles of the following steps: 95°C for 20 seconds, 60°C for 20 seconds, and 72°C for 30 seconds. Primer sequences, primer amplification efficiencies, and product sizes are listed in Tables S1 and S4. Data normalized to HPRT1 are presented in Table S3. Fold changes calculated for every well for each gene were pooled from three biological replicates and plotted as box plot using GraphPad Prism 8. Median values are represented by lines in the boxplots, whereas means are represented by a plus sign inside the box. Three biological replicates were used. Whisker setting: Min to Max, show all points.

2.8 | TaqMan microRNA assay

Expression of miR-137 was quantified using cDNA and TaqMan microRNA assay (001129, Applied Biosystems) that includes specific RT primers and TaqMan probes. RNU48, small nucleolar RNA (001006), was used as an internal control for normalization and analysis was performed as described in Supporting Information.

2.9 | Mitochondrial DNA quantitation

cDNA was prepared from RNA extracted from transfected cells using High-Capacity cDNA Reverse Transcription Kit according to

manufacturer's instructions (Applied Biosystems). Quantitative RT-PCR was performed for succinate dehydrogenase complex subunit A (SDHA, nuclear encoded) and NADH dehydrogenase 5 (ND5, mitochondrial encoded) in triplicate and repeated three times. The relative expression ratio of the mitochondrial ND5 to the nuclear SDHA was calculated. Relative mtDNA content was measured by the $\Delta\Delta C_t$ method.³⁸ Primer sequences are listed in Table S1.

2.10 | Oxygen consumption rate measurements

Oxygen consumption rate (OCR) was measured in hiNSCs using Seahorse XFe24 Extracellular Flux Analyzer (Seahorse Biosciences/Agilent Technologies, Santa Clara, California). hiNSCs were seeded in NSC media in matrigel-coated Seahorse XF 24 microplate (Seahorse Biosciences) at a density of 0.75×10^5 cells/well to ensure about 90% confluency at the time of OCR measurement leaving A1, B4, C3, and D6 wells blank. This assay is detailed in Supporting Information.

2.11 | Western blotting

5×10^5 transfected cells were lysed as described³⁹ with modified RIPA buffer (50 mM Tris-HCl, pH 7.4; 150 mM NaCl, 1% NP40, 0.25% Na-deoxycholate, 1 mM EDTA) containing protease inhibitor cocktail (Sigma-Aldrich) and 0.2% sodium orthovanadate. An equal amount of protein (30 μ g) from each transfected group was separated on 10%-12% SDS polyacrylamide gel and transferred to PVDF membrane (Mdi; Advanced Microdevices Pvt. Ltd., India). The membranes were incubated with antibodies and images were captured as described in Supporting Information.³⁹ Representative blots are shown in figures.

2.12 | Cell proliferation assessment using Ki67

50 000 cells/well were seeded in permanox four-well chamber slides 1 day prior to transfection. After 24 hours of transfection with miR-137 mimic or inhibitor, cells were washed with 1X PBS followed by fixation with 4% paraformaldehyde for 20 minutes in dark and washed with 1X PBS thrice. Blocking and permeabilization were performed with 4% bovine serum albumin (BSA) and 0.3% Triton X-100 in PBS. Cells were incubated with primary antibody anti-Ki67 (1:1000, Abcam, Ab16667, Cambridge, UK) overnight at 4°C. After washing, cells were incubated with Alexa Flour tagged 594 (1:1000) secondary antibody for 1 hour at room temperature. Subsequently, cells were mounted using ProLong Gold Antifade Reagent with DAPI (Invitrogen). Fluorescent images were captured using Axiolmager.Z1 microscope at $\times 20$ objective at room temperature. For analysis, a minimum of 10 images were captured from random fields in each group. The persons who captured the images, counted the cells, and performed further analysis were blinded to the experimental groups. Double positive cells for Ki67 and DAPI were counted using ImageJ software. The mean of double positive cells for Ki67

and DAPI was calculated from 10 random visual fields from three biological replicates ($n = 3$) and plotted on a logarithmic scale.

2.13 | Immunocytochemistry

This assay is detailed in Supporting Information.

2.14 | Fluorescent imaging for mitochondrial biogenesis

Live cell microscopy was performed by Leica DMI6000 inverted fluorescent microscope (Leica Germany). Briefly, 50 000 hiNSCs were seeded per well of four-well chambered glass slides (Labtek, Thermo Scientific) 1 day prior to transfection. After 24 hours of transfection with miR-137 mimic or inhibitor, cells were washed with 1X PBS followed by staining with Mitotracker Green FM (400 nM, Invitrogen) for 15 minutes in dark at 37°C and washed with 1X PBS twice. Live cells were observed under the Leica microscope DMI6000 with a $\times 63$ at room temperature.

3 | STATISTICAL ANALYSIS

Data from three independent experiments were presented as mean \pm SD. A minimum of three biological replicates ($n = 3$) were used for each data set. For statistical analysis, the data were analyzed by one-way ANOVA followed by Tukey's post hoc test. P value $< .05$ was considered significant.

4 | RESULTS

4.1 | MiR-137 decreases proliferation of hiNSCs

To examine whether miR-137 has any role in hiNSC's fate determination, we induced NSCs from human iPSCs and termed them hiNSCs. These hiNSCs stained positive for NSC markers, SOX2 and Nestin (Supplementary Figure S1). We transfected hiNSCs with mature miR-137 mimic and inhibitor as described in methods. After 24 hours of transfection, cell proliferation was assessed by immunostaining with the Ki67 antibody.⁴⁰ Transfection of miR-137 (40 nM) in hiNSCs substantially reduced the number of Ki67-positive cells as compared to the NC (Figure 1A,B). Inhibition of miR-137 by anti-miR-137 abolished its impact on proliferation and significantly increased the number of Ki67-positive cells (Figure 1A,B). This result indicates that miR-137 decreases proliferation of hiNSCs.

4.2 | MiR-137 accelerates differentiation of hiNSCs

Termination of cell proliferation is concomitant to differentiation, subsequently we questioned whether miR-137 impacts differentiation of

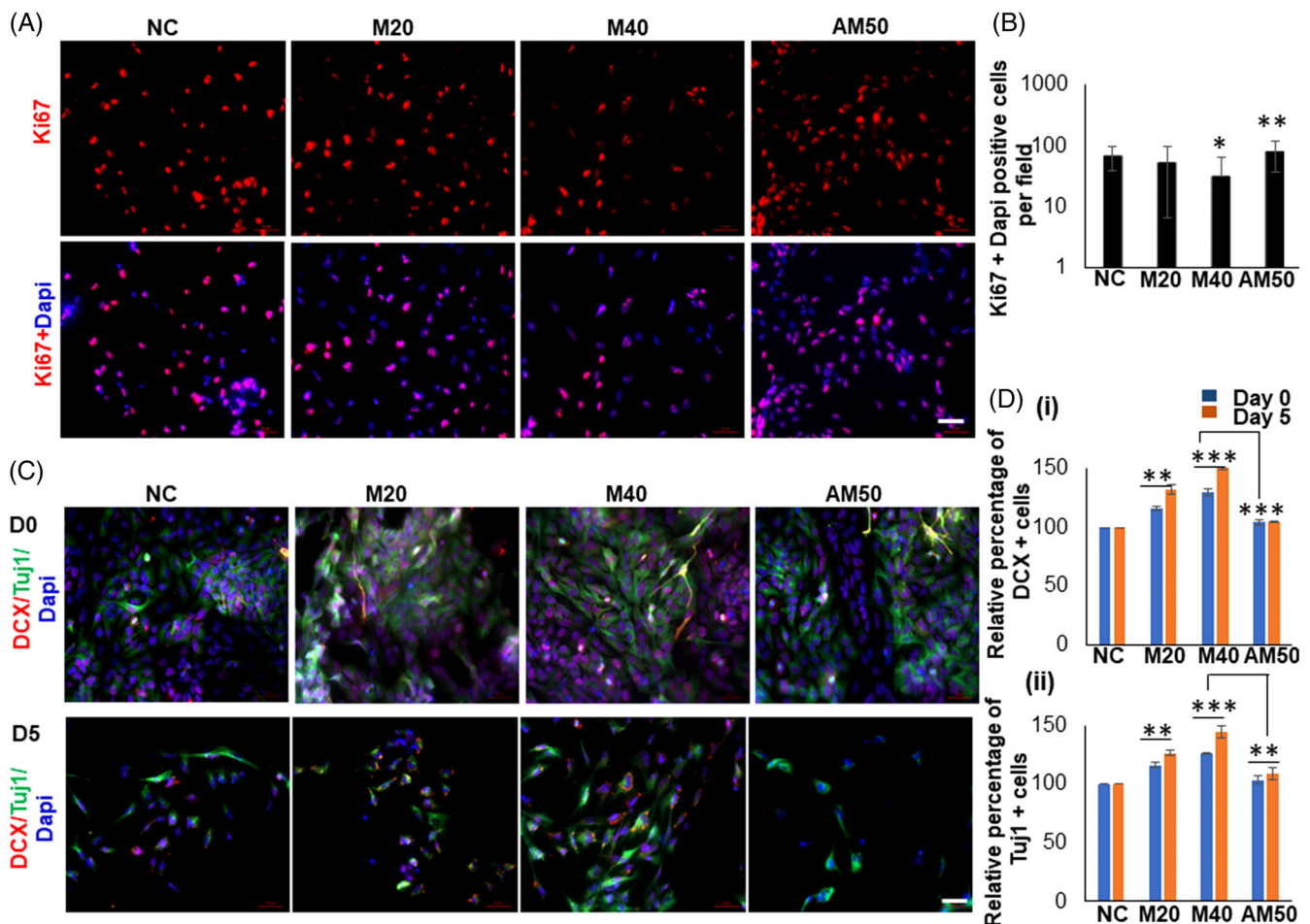


FIGURE 1 MiR-137 reduces the proliferation and increases the differentiation of induced neural stem cells (hiNSCs). A, hiNSCs transfected either with negative control (NC) or with miR-137 mimic at 20 or 40 nM or with 50 nM anti-miR-137 (AM50) and immunostained with Ki67, proliferation marker (red), and DAPI for nucleus (blue) 24 hours post-transfection. Representative immunocytochemistry images of the hiNSCs have been shown from three biological replicates ($n = 3$). Scale bar = 50 μm . B, Bar diagram represents the mean of double positive cells for Ki67 and DAPI that was calculated from 10 random visual fields from three biological replicates. The values on the bar graph represent the mean \pm SD of three biological replicates ($n = 3$); * $P < .05$ in comparison to negative control, ** $P < .01$ in comparison to miR-137 (40 nM)-transfected group. C, hiNSCs transfected either with NC or with miR-137 mimic at 20 or 40 nM or with 50 nM anti-miR-137 were differentiated in neural differentiation medium until day 5. Transfected cells were immunostained with TUJ1 (green, for newly formed neurons), DCX (red, as early marker for neurogenesis), and DAPI (blue, for nucleus) at day 0 and day 5. Representative immunocytochemistry images of the differentiated cells have been shown from three biological replicates ($n = 3$). Scale bar = 50 μm . D, Bar graph represents the relative percentage of TUJ1 and DCX positive cells over DAPI in the indicated groups. The values on the bar graph correspond to mean \pm SD of three biological replicates ($n = 3$). ** $P < .01$ and *** $P < .001$. AM50, 50 nM of anti-miR-137; M20, 20 nM of miR-137 mimic; M40, 40 nM of miR-137 mimic

hiNSCs. We transfected hiNSCs with mature miR-137 mimic and inhibitor and differentiated them into neurons until day 5 as described in methods. Ectopic expression of miR-137 in hiNSCs led to a significant increase in percentage of cells expressing DCX and TUJ1 (early markers for neurogenesis and newly formed neurons, respectively) from day 0 to day 5 of differentiation (Figure 1C,D). However, anti-miR-137 reduced percentage of cells expressing DCX and TUJ1 during differentiation (Figure 1C,D). Addition of 20 and 40 nM of miR-137 in hiNSCs increased punctate expression of DCX by $33\% \pm 2.8\%$ and $53\% \pm 2.3\%$, respectively, at fifth day of differentiation. Anti-miR-137, however, reduced the differentiation close to normal range (Figure 1D). Concordantly, in miR-137-transfected hiNSCs, the

percentage of TUJ1 positive cells were increased to 26% and 44% at the mentioned concentrations as compared to the NC, while reduced significantly in anti-miR-137-transfected cells (Figure 1D).

To verify the effect of miR-137 on differentiation, we assessed transcript levels of the pro-neural (ROBO2, SPOCK1, and DCX), neuronal (TUJ1 and MAP2), and astrocytic (GFAP) markers in presence of miR-137 mimic.^{35,41} The transcript levels of ROBO2, SPOCK1, and DCX were robustly increased to 2.1 ± 0.6 , 2.2 ± 0.3 , and 2.4 ± 0.4 -fold (mean \pm SD, $n = 3$), respectively, at 40 nM concentration of miR-137 mimic with respect to NC (Figure 2Ai-iii). A significant increase in mRNA levels of neuronal markers, TUJ1, MAP2, and ASCL1 was observed at 40 nM concentration of miR-137

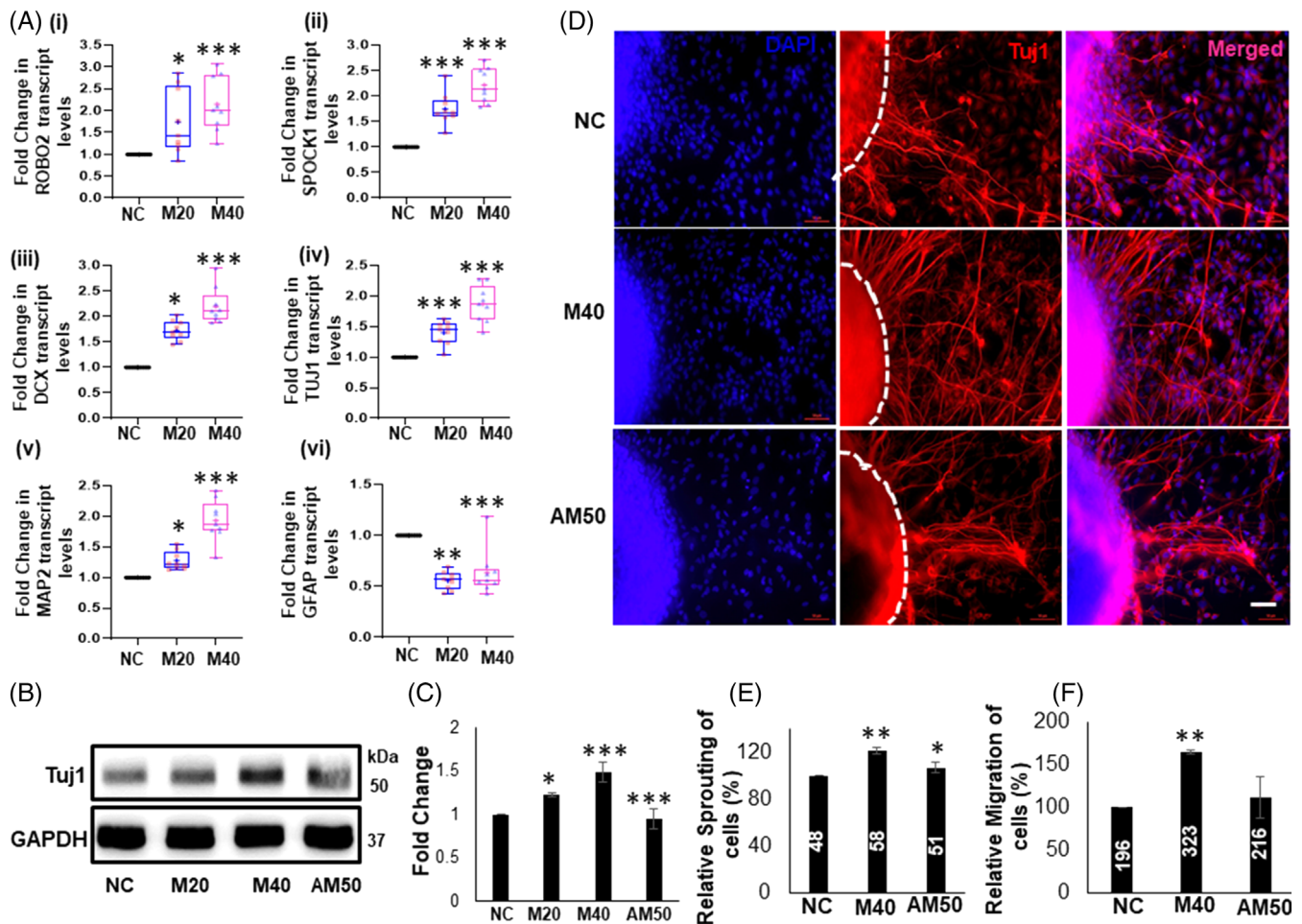


FIGURE 2 MiR-137 enhances neuronal differentiation and migration. A(i)-(vi), Real-time PCR for pro-neuronal markers (ROBO2, SPOCK1, DCX) (i-iii), neuronal markers (TUJ1, MAP2) and an astrocyte marker (GFAP) (iv-vi) 24 hours post-transfection in the negative control (NC) or miR-137 mimic (20 or 40 nM) transfected hiNSCs. RPL13A was used for the normalization. Median values are represented by lines in the boxplots, whereas means are represented by a plus sign inside the box. Three biological replicates were used. B, Representative image of Western blot of TUJ1 protein expression in hiNSCs transfected with NC or miR-137 mimic (20 or 40 nM) or with 50 nM anti-miR-137 (AM50) after 24 hours of transfection. GAPDH served as a loading control. Representative blots from three biological replicates have been shown. C, Bar diagram represents the mean fold change calculated with respect to negative control after integrated densitometric values normalized to GAPDH from three biological replicates. D, hiNSCs transfected either with negative control or with miR-137 mimic (40 nM) or with 50 nM anti-miR-137 (AM50) were allowed to form neurospheres as described in methods. Representative micrographs from three biological replicates ($n = 3$) show the neurons migrating from adherent neurospheres after immunostaining with TUJ1 (red) and DAPI (blue). Scale bar = 50 μ m. E, F, For each experimental group, a minimum of five similar-sized neurospheres were imaged on Axiolmager.Z1 microscope (Carl Zeiss) from 3 biological replicates. E, For sprouting assay, the number of neurites per neurosphere were counted using ImageJ software in three randomly chosen fields. Bar graph (E) represents relative percentage of neurons sprouting from neurospheres which is computed by averaging the number of neurites for each experimental group. The average number of neurites from all neurospheres is also indicated on the bar graph for each treatment type. F, For migration assay, neurite length was traced from the periphery of the neurosphere using line tool in ImageJ software and three random measurements were obtained per neurosphere. Bar graph (F) represents relative percentage of migration of neurons from periphery of neurospheres which is computed by averaging length measurements for each experimental group. The average length of neurites from all neurospheres is also mentioned on the bar graph for each treatment type. Length of the neurite corresponds to distance travelled by the neurite. For (C-F), the values represent the mean \pm SD from three biological replicates ($n = 3$). For all panels, * $P < .05$, ** $P < .01$, and *** $P < .001$. AM50, 50 nM of anti-miR-137; M20, 20 nM of miR-137 mimic; M40, 40 nM of miR-137 mimic

mimic (Figure 2Aiv,v; Figure S2A). Nevertheless, we noticed a significant decline in the transcript levels of GFAP (astrocytic marker) by 1.7 ± 0.2 -fold in presence of miR-137 (40 nM) (Figure 2Avi). Protein levels of TUJ1 were increased to 1.5-fold in 40 nM miR-137

mimic expressing hiNSCs as compared to NC. However, anti-miR-137 reduced TUJ1 protein levels significantly and abolished miR-137 effect (Figure 2B,C). Thus, these results suggest that miR-137 promotes neuronal differentiation of hiNSCs.

4.3 | MiR-137 alters migration of neurons

Migration of neurons is an essential process for neural development.⁴² The neurospheres represent an ideal in vitro model system for studying migration of neurons. The neurospheres formed from transfected hiNSCs were seeded onto PDL-coated surface, cultured in neuronal differentiation media, and migration of cells was assessed as described in methods. As evident from Figure 2D-F, sprouting and migration of neurons from neurospheres were accelerated in miR-137 mimic transfected neurospheres by $21\% \pm 2.1\%$ and by $65\% \pm 1.7\%$ as compared to NC, respectively. However, in presence of anti-miR-137, sprouting

and migration of neurons were restored close to control range (Figure 2D-F). These results suggest that miR-137 increases neuronal migration.

4.4 | MiR-137 represses MEF2A expression by targeting its 3'UTR

To uncover the underlying mechanism of miR-137 mediated effects, we examined the targets of miR-137 using TargetScan⁴³ and microT-CDS⁴⁴ algorithms. Potential binding sites of miR-137 were found in 3'UTR of

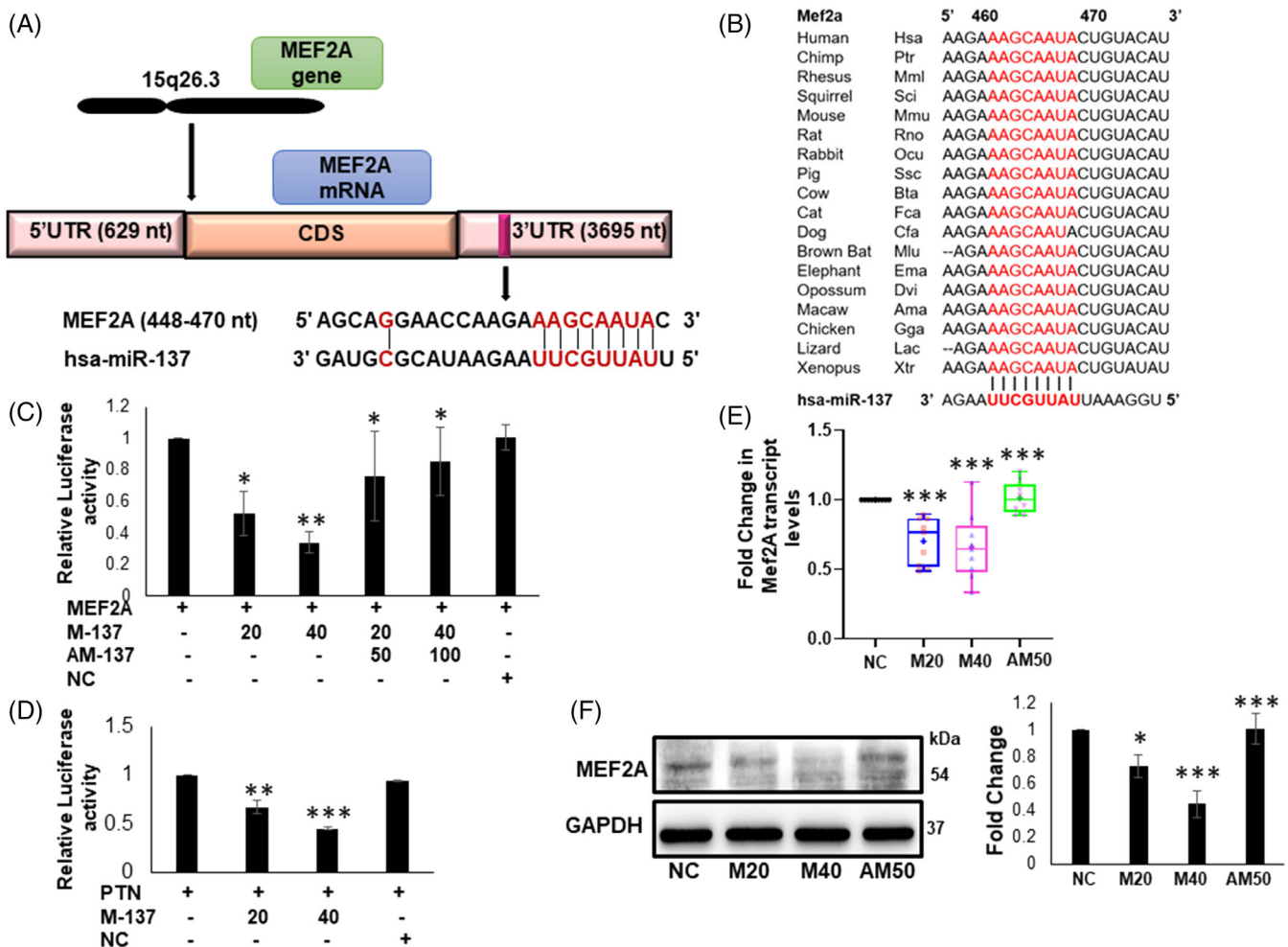


FIGURE 3 MiR-137 targets 3'UTR of MEF2A. A, Schematic diagram showing the MEF2A gene and its 3'UTR. Complete complementarity between 2 and 9 nucleotides of miR-137 and its predicted binding site in 3'UTR of MEF2A gene has been shown (red color). B, Binding site of miR-137 in the 3'UTR of MEF2A gene is highly conserved among various mammalian species as predicted by TargetScan 7. C, D, HEK293 cells were co-transfected with pMIR-REPORT-MEF2A 3'UTR construct and/or miR-137 mimic or anti-miR-137 at 50 or 100 nM or negative control. The luciferase activity was measured 24 hours post-transfection, normalized to Renilla luciferase, and was plotted relative to pMIR-REPORT-MEF2A 3'UTR (C). Luciferase assay using PTN reporter vector was used as a positive control experiment (D). E, qRT-PCR analysis of MEF2A transcript levels in the presence of miR-137 and anti-miR-137. RPL13A was used as normalization control. Median values are represented by lines in the boxplots, whereas means are represented by a plus sign inside the box. Three biological replicates were used. F, Representative image of Western blot of MEF2A from hiNSCs 24 hours post-transfection of negative control or miR-137 mimic (20 or 40 nM) or anti-miR-137 (50 nM) is shown. GAPDH served as a loading control. Right panel show bar diagram that depicts the mean fold change calculated with respect to negative control after integrated densitometric values normalized to GAPDH. Data expressed in (C-F) are from three biological replicates and (C-D, F) presented as mean \pm SD of three independent experiments; * $P < .05$, ** $P < .01$, *** $P < .001$. AM50, 50 nM of anti-miR-137; M20, 20 nM of miR-137 mimic; M40, 40 nM of miR-137 mimic; NC, negative control

MEF2A (Figure 3A). The complete complementarity between 2- and 8-nt of seed region of mature miR-137 and 463-469 nt of 3'UTR of MEF2A was observed (Figure 3A). The binding site was found to be conserved across various mammalian species as revealed by multiple sequence alignment (Figure 3B). We cloned human MEF2A 3'UTR containing the predicted miR-137 binding site in pMIR-REPORT Vector and transfected in HEK293 cells. Luciferase activity was measured as described in methods. Specifically, luciferase activity reduced to $48\% \pm 8\%$ and $66\% \pm 4.1\%$ (Figure 3C) in miR-137-transfected groups at 20 and 40 nM, respectively, as compared to NC. However, anti-miR-137 relieved the repression as shown by a significant increase in luciferase activity in comparison to miR-137 mimic (Figure 3C). Pleiotrophin (PTN) was used as a positive control

for the experiment (Figure 3D).⁴⁵ These results suggest that miR-137 represses MEF2A expression by binding to its 3'UTR.

To verify whether miR-137 regulates MEF2A at post-transcriptional levels, we determined transcript and protein levels of MEF2A in miR-137-transfected cells. MiR-137 (at 40 nM) significantly reduced the transcript levels of MEF2A, while anti-miR-137 increased MEF2A transcript levels (Figure 3E). Protein levels of MEF2A were diminished by 1.4 ± 0.1 -fold and 2.2 ± 0.1 -fold in miR-137-transfected cells at both concentrations, respectively (Figure 3F). However, anti-miR-137 markedly increased the MEF2A protein levels by 2.3 ± 0.1 -fold as compared to mimic (40 nM) (Figure 3F). Thus, these results suggest that miR-137 reduces endogenous MEF2A expression in hiNSCs.

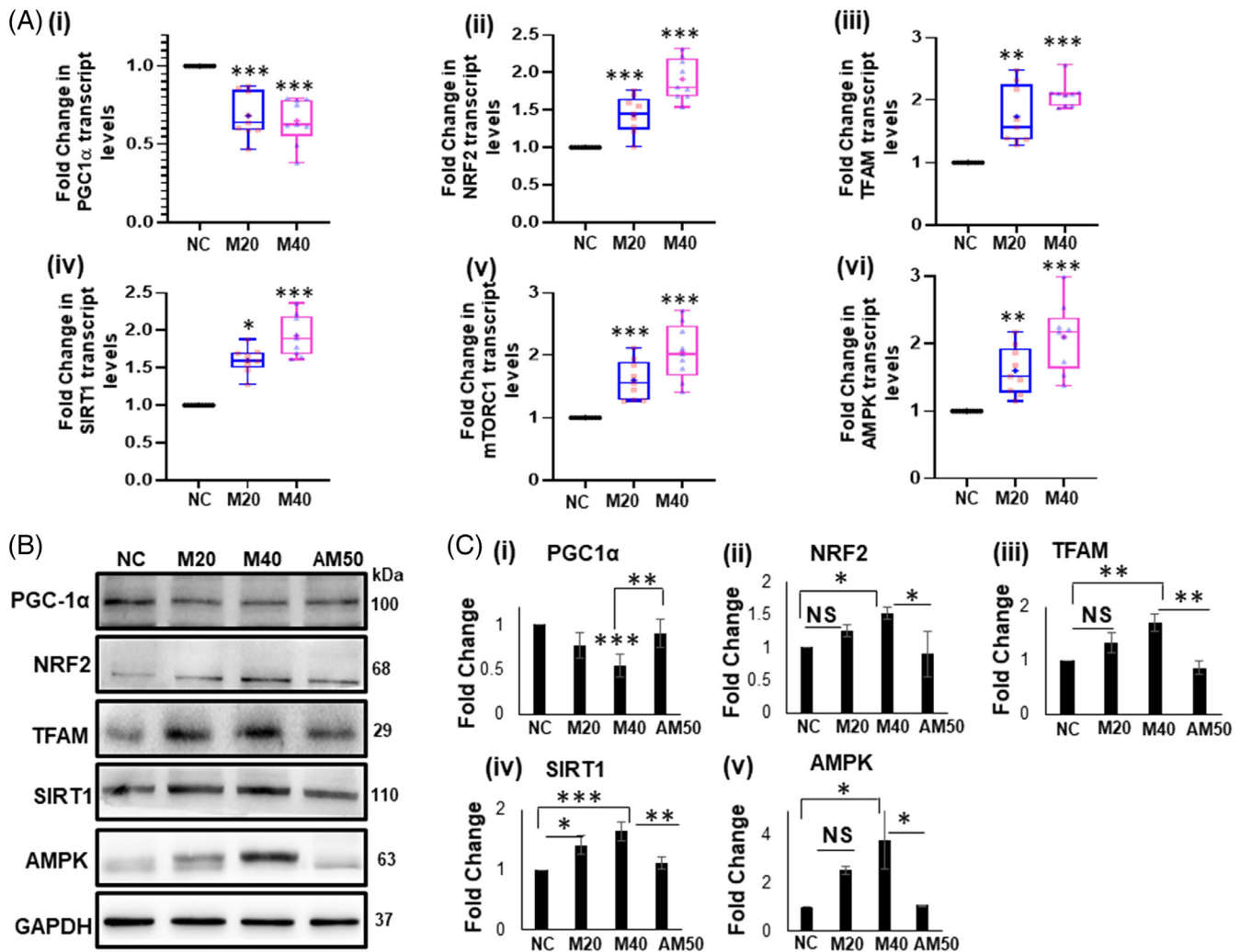


FIGURE 4 MiR-137 induces the mitochondrial biogenesis. A(i-vi) qRT-PCR analysis of transcript levels of molecular regulators of mitochondrial biogenesis (PGC1 α , NRF2, TFAM, SIRT1, mTOR, and AMPK) in hiNSCs transfected either with negative control or miR-137 mimic (20 or 40 nM). RPL13A was used as normalization control. Median values are represented by lines in the boxplots, whereas means are represented by a plus sign inside the box. Three biological replicates were used. * $P < .05$, ** $P < .01$, *** $P < .001$. B, Representative images of Western blot of protein levels of different genes from hiNSCs, 24 hours post-transfection of negative control or miR-137 mimic (20 or 40 nM) or anti-miR-137 (AM50) are shown. GAPDH served as a loading control. C(i-v), Bar diagram represents the mean fold change calculated with respect to negative control after integrated densitometric values normalized to GAPDH from three biological replicates ($n = 3$), mean \pm SD; * $P < .05$, ** $P < .01$, *** $P < .001$. AM50, 50 nM of anti-miR-137; M20, 20 nM of miR-137 mimic; M40, 40 nM of miR-137 mimic; NC, negative control; NS, nonsignificant

4.5 | MiR-137 induces mitochondrial biogenesis in hiNSCs

MEF2A, being a transcriptional regulator of PGC1 α , led us to examine whether miR-137 modulates mitochondrial biogenesis to achieve enhanced neuronal differentiation. We evaluated transcript levels of key regulators associated with mitochondrial biogenesis in miR-137-transfected hiNSCs. Of these, PGC1 α is the master regulator of mitochondrial biogenesis.⁴⁶ Surprisingly, mRNA levels of PGC1 α reduced significantly in miR-137 mimic transfected cells (Figure 4Ai). PGC1 α activates downstream molecules including nuclear respiratory factor (NRF) to initiate mitochondrial biogenesis.⁴⁷ Despite reduced mRNA levels of PGC1 α , notably, miR-137 caused a striking increase in the transcript levels of NRF2 (Figure 4Aii). NRF2 further promotes expression of nuclear genes that encode for mitochondrial proteins such as transcription factor A of mitochondria (TFAM).⁴⁸ Furthermore, we observed elevated mRNA levels of TFAM in miR-137 mimic transfected hiNSCs (Figure 4Aiii). To elucidate upstream regulators of mitochondrial biogenesis involved in miR-137-mediated modulation, we assessed the transcript levels of SIRT1, mTORC1, and AMPK.⁴⁹⁻⁵² Increase in the

transcript levels of SIRT1, mTORC1, and AMPK was evident in miR-137-transfected hiNSCs (Figure 4Aiv,vi).

To determine the impact of miR-137 on protein levels of these genes, we performed Western blot. In concordance with transcript levels, the protein levels of PGC1 α were diminished by 1.8-fold in miR-137 mimic (40 nM) transfected hiNSCs and increased significantly in presence of anti-miR-137 (Figure 4B,Ci). The expression of NRF2, TFAM, SIRT1, and AMPK increased significantly in miR-137 mimic (40 nM) transfected hiNSCs and anti-miR-137 abolished the effect of miR-137 on these genes (Figure 4B,Cii-iv). Thus, these results indicate that miR-137 plays an essential role in mitochondrial biogenesis by regulating its key molecular regulators.

4.6 | MiR-137 modulates mitochondrial fusion and fission in hiNSCs

Mitochondrial biogenesis along with fusion and fission maintains mitochondrial homeostasis⁵³; therefore, we investigated the impact of

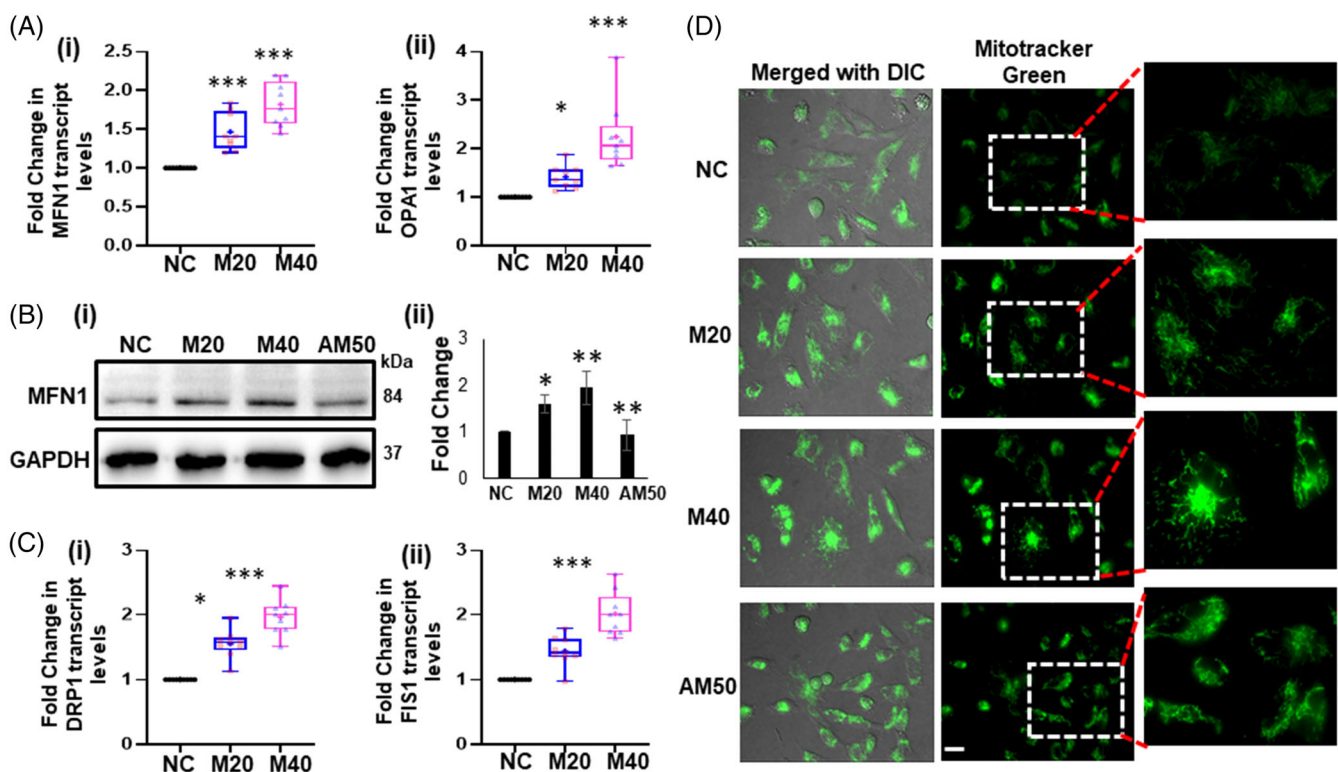


FIGURE 5 MiR-137 affects mitochondrial fusion and fission. A, qRT-PCR analysis of transcript levels of mitochondrial fusion regulators MFN1 and OPA1 after transfection of miR-137 mimic in hiNSCs at 20 and 40 nM concentrations. Data are normalized to RPL13A. Median values are represented by lines in the boxplots, whereas means are represented by a plus sign inside the box. Three biological replicates were used. B, Representative image of Western blot of MFN1 protein levels in presence of miR-137 mimic at 20 and 40 nM and anti-miR-137 at 50 nM is shown. GAPDH was used as a loading control. The right panel shows the bar diagram that represents the fold change calculated with respect to negative control after integrated densitometric values normalized to GAPDH. Data shown are from three biological replicates ($n = 3$, mean \pm SD). C, qRT-PCR analysis represents the increased transcript levels of mitochondrial fission genes DRP1 and FIS1 after transfection of miR-137 mimic in hiNSCs. RPL13A was used as normalization control. * $P < .05$, ** $P < .01$, *** $P < .001$. AM50, 50 nM of anti-miR-137; M20, 20 nM of miR-137 mimic; M40, 40 nM of miR-137 mimic; NC, negative control. D, Representative images of mitochondria in hiNSCs labeled with MitoTracker Green post 24 hours of transfection from three biological replicates. Enlarged view in the inset of "MitoTracker" panel shows accumulation of more mitochondria as seen by increased fluorescence intensity of MitoTracker Green in the miR-137 mimic transfected hiNSCs (20 and 40 nM) relative to negative control. Scale bar = 20 μ m, $n = 3$

miR-137 on mitochondria fusion and fission. Transcript and protein levels of key regulators of mitochondrial fusion (mitofusin 1 [MFN1], mitofusin 2 [MFN2], and optic atrophy protein 1 [OPA1]) and fission (dynamin related protein 1 [DRP1] and mitochondrial fission 1 [FIS1]) were evaluated in the presence of miR-137. Substantial increase in the transcript levels of MFN1, MFN2, and OPA1 was evident in miR-137 (40 nM)-transfected hiNSCs (Figure 5Ai,ii; Figure S2B). Protein levels of MFN1 were increased to 1.9 ± 0.2 -fold in miR-137 mimic (40 nM) transfected cells and reduced significantly in presence of anti-miR-137 (Figure 5Bi,ii). MiR-137 also increased the transcript levels of DRP1 and FIS1 to 2.0 ± 0.3 -fold and 2.3 ± 0.5 -fold, (mean

\pm SD, $n = 3$), respectively (Figure 5Ci,ii). These results suggest that miR-137 enhances mitochondrial fusion and fission in hiNSCs to accelerate neuronal maturation.

4.7 | MiR-137 regulates mitochondrial dynamics and activates OXPHOS

MiR-137 modulated mitochondrial biogenesis, fusion, and fission in hiNSCs (Figures 4 and 5C); therefore, we determined the mitochondrial content by staining transfected hiNSCs with MitoTracker Green as

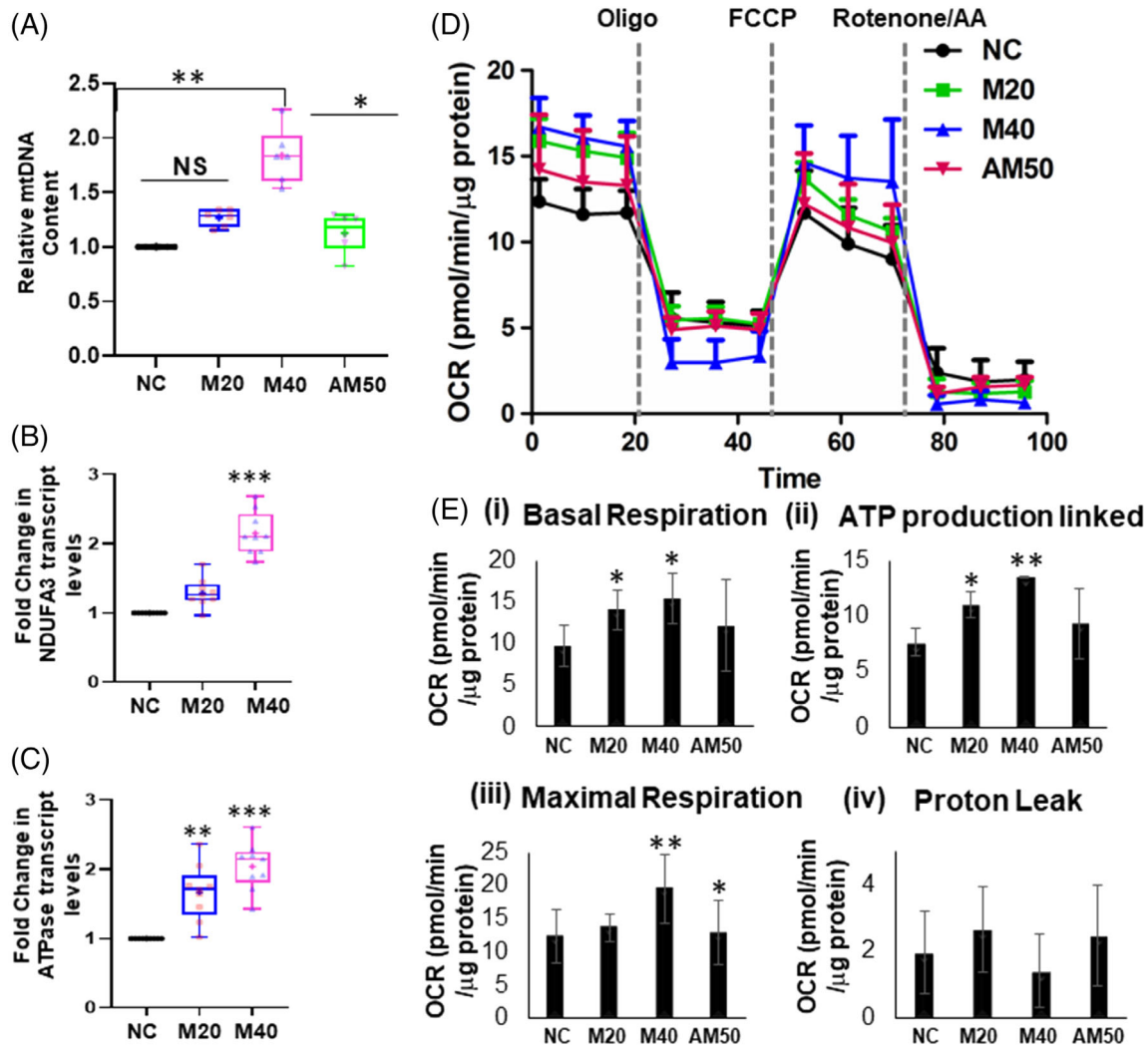


FIGURE 6 MiR-137 increases mitochondria content and activates OXPHOS. A, Quantification of relative mitochondrial DNA copy numbers measured by qRT-PCR of mitochondrial ND5 gene and normalized against the nuclear SDHA gene. The increase in mtDNA/nDNA ratio in miR-137 mimic transfected hiNSCs is indicative of the increased mtDNA copy number. B,C, qRT-PCR of transcript levels of NDUFA3 (Complex I) and ATPase V (Complex V) of ETC in hiNSCs transfected with miR-137 mimic at 20 or 40 nM as compared to negative control. RPL13A was used as normalization control. Median values are represented by lines in the boxplots, whereas means are represented by a plus sign inside the box. In (A-C), three biological replicates were used. D, The OCR in transfected hiNSCs was measured as a function of time. Oligomycin ($1 \mu\text{M}$) or FCCP ($2 \mu\text{M}$), or rotenone/antimycin A (AA) ($1 \mu\text{M}$) were added at the indicated time points. To show relevant differences, only upper error bars have been plotted. E, Bar graph corresponding to the calculation of basal, ATP-linked, maximal, and proton-leak associated OCR in transfected hiNSCs. Bar graph for basal respiration depicts mean of OCR from 1 to 18.5 minutes after subtracting nonmitochondrial respiration. Nonmitochondrial respiration is subtracted to calculate other parameters also. The data are obtained from two biological replicates and plotted as mean \pm SD. For all panels, * $P < .05$, ** $P < .01$, *** $P < .001$. AM50, 50 nM of anti-miR-137; M20, 20 nM of miR-137 mimic; M40, 40 nM of miR-137 mimic; NC, negative control

described in methods. In the presence of miR-137, the mitochondrial content increased significantly as indicated by increased fluorescence intensity of MitoTracker Green at both concentrations (20 and 40 nM) (Figure 5D). However, anti-miR-137 reduced the mitochondrial content as fluorescence intensity of MitoTracker Green diminished relative to miR-137 (40 nM)-transfected cells (Figure 5D). To verify this, we assessed the relative mitochondrial (mt) DNA content by qRT-PCR. In agreement with Figure 5D, the ratio of mitochondrial ND5 gene to nuclear SDHA gene revealed an increase in mtDNA content by 1.9 ± 0.2 -fold in miR-137 (40 nM)-transfected hiNSCs (Figure 6A). However, reduced mtDNA content is evident in anti-miR-137-transfected hiNSCs (Figure 6A). We conclude that miR-137 increases mitochondrial content.

To examine whether increase in mitochondrial content is associated with activation of OXPHOS, we assessed mRNA levels of subunits of different complexes of the electron transport chain (ETC) after ectopic expression of miR-137 in hiNSCs. miR-137 significantly increased the

transcript levels of NADH:Ubiquinone Oxidoreductase Subunit A3 (NDUFA3, subunit of Complex I), Mitochondrial membrane ATP synthase (F1FO ATP synthase or Complex V), and Succinate Dehydrogenase Complex Iron Sulfur Subunit B (SDHB, subunit of Complex II) (Figure 6B,C; Figure S2C). To verify acceleration of OXPHOS, we characterized bioenergetic profiles of miR-137-transfected hiNSCs by evaluating OCR. Enhanced basal respiration levels were evident in miR-137-transfected hiNSCs, while they were diminished in anti-miR-137-transfected cells (Figure 6D,Ei). Treatment of oligomycin, inhibitor of ATP synthase, induced greater loss of OCR in miR-137 (40 nM)-transfected hiNSCs; however, the loss was rescued in anti-miR-137-transfected hiNSCs (Figure 6Eii). Greater loss of OCR during oligomycin treatment in miR-137-transfected hiNSCs indicated a high level of mitochondrial respiration was coupled with ATP production (Figure 6D,Eii). Nonsignificant reduction in proton leak and a significant increase in maximal respiration was observed in miR-137-transfected hiNSCs

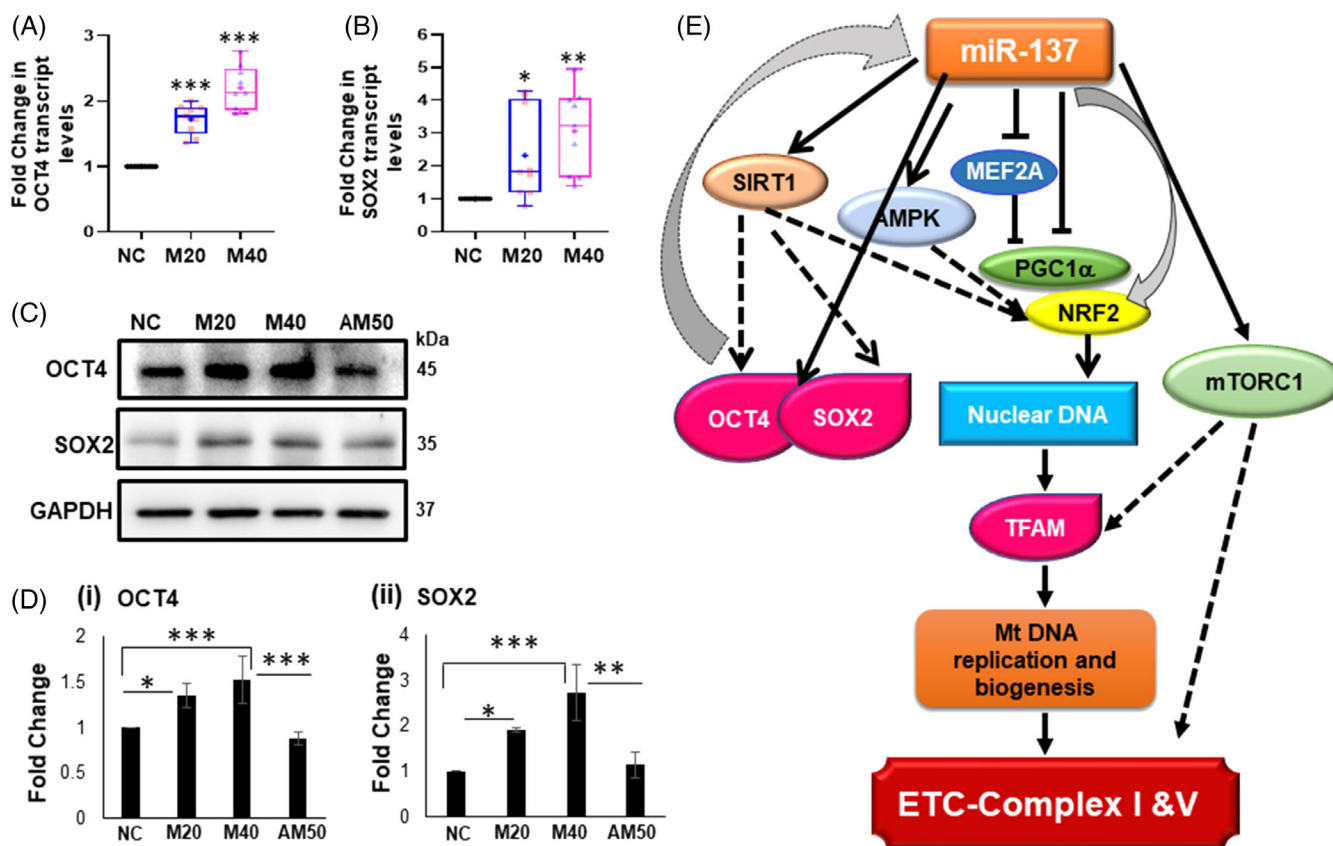


FIGURE 7 MiR-137 modulates pluripotency factors OCT4 and SOX2. A,B, qRT-PCR analysis of transcript levels of pluripotency factors OCT4 and SOX2 after transfection of miR-137 mimic in hiNSCs at 20 and 40 nM concentrations. Data are normalized to RPL13A. Median values are represented by lines in the boxplots, whereas means are represented by a plus sign inside the box. Three biological replicates were used. C, Representative images of Western blot of protein levels of OCT4 and SOX2 from hiNSCs, 24 hours post-transfection of negative control or miR-137 mimic (20 or 40 nM) or anti-miR-137 (50 nM) are shown. GAPDH served as a loading control. D, Bar diagrams depict the mean fold change calculated with respect to negative control after integrated densitometric values normalized to GAPDH from three biological replicates. Data are expressed as mean \pm SD of three independent experiments; * $P < .05$, ** $P < .01$, *** $P < .001$. M20, 20 nM of miR-137 mimic; M40, 40 nM of miR-137 mimic; NC, negative control. E, Proposed model of regulation of mitochondrial dynamics by miR-137: Our data show that miR-137 mediated activation of SIRT1, AMPK, NRF2, and TFAM and inhibition of MEF2A and PGC1 α may be responsible for induction of mitochondrial biogenesis and activation of OXPHOS in hiNSCs. SIRT1 might increase OCT4 and SOX2 expression which in turn enhances the transcription of miR-137, thus establishes a feed-forward self-regulatory loop. Dotted lines indicate that these have been demonstrated in the previous studies

(Figure 6D,Eiii,iv). Increase in maximal respiration indicated higher maximal respiratory capacity of mitochondria in miR-137-transfected hiNSCs. However, maximal respiration was decreased in presence of anti-miR-137. Final treatment of rotenone/antimycin A demonstrated a nonsignificant reduction in OCR due to nonmitochondrial sources in miR-137-transfected hiNSCs which further strengthen our observation that mitochondrial respiration was more prevalent in miR-137-transfected hiNSCs (Figure S3A). Our results are in harmony with previous studies showing higher mitochondrial respiration during cell differentiation.^{54,55} Collectively, these results indicate that miR-137 activates OXPHOS by inducing mitochondrial respiration in hiNSCs.

4.8 | MiR-137 modulates transcription factors OCT4 and SOX2

The promoter of miR-137 gene is co-occupied by the key pluripotency transcription factors, OCT4 and SOX2,¹⁰ therefore, we questioned whether miR-137 has any regulatory effect on OCT4 and SOX2. We quantified the mRNA and protein levels of OCT4 and SOX2 after ectopic expression of miR-137 in hiNSCs. miR-137 markedly increased the transcript levels of OCT4 and SOX2 by 2.2 ± 0.3 -fold and 3.1 ± 1.3 -fold (mean \pm SD, $n = 3$), respectively (Figure 7A,B). Significant elevation of protein levels of OCT4 and SOX2 by 1.5 ± 0.2 -fold and 2.7 ± 0.4 -fold was evident in miR-137 (40 nM)-transfected hiNSCs (Figure 7C,D). Addition of anti-miR-137 significantly reduced protein levels of these genes (Figure 7C,D). These results indicate positive regulation of OCT4 and SOX2 by miR-137.

5 | DISCUSSION

The design and execution of stem cell-based therapies for neurological diseases require a fundamental understanding of human neural development.⁵⁶ NSC fate determination is an important process during neural development that determines terminal-cell fates and organization of cells in the brain.⁵⁷ Recent technological development of stem cell field has permitted derivation of human NSCs from iPSCs, which represent a remarkable *in vitro* model to study neural development and neurological diseases. Posttranscriptional regulators including miRNAs modulate neural development at distinct stages. To understand the role of miR-137 in human NSCs fate determination, we modulated miR-137 expression levels in hiNSCs derived from human iPSCs. Here, we showed that miR-137 inhibited hiNSC proliferation and enhanced neuronal differentiation. Our study also elucidated possible molecular mechanism by which miR-137 modulates hiNSCs fate.

Our study is in harmony with other reports, which are based on mouse models and show that miR-137 inhibits proliferation of embryonic and adult subventricular zone-derived NSCs and enhances their differentiation.^{18,22} In contrast, during adult neurogenesis, miR-137 has been shown to enhance proliferation and reduce differentiation of adult hippocampal derived NSCs.⁵⁸ These contradictory results point to the cellular context dependent function of miR-137 in NSCs.

The role of miR-137 is also evident in modulating hippocampal neuronal maturation.^{58,59} To the best of our knowledge, no evidence on these observations is available in humans; however, our system would permit such investigations.

We put forward a hypothetical model to explain modulation of mitochondrial dynamics by miR-137 based on our current results and previous studies. In our study, ectopic expression of miR-137 in hiNSCs increased SIRT1, OCT4, and SOX2 expression (Figures 4A,B and 7A-D). OCT4 and SOX2 are regulated by SIRT1, which might activate these genes.^{60,61} Furthermore, OCT4 and SOX2 harbor binding sites in the promoter region of miR-137 gene, therefore, increased expression of OCT4 and SOX2 might activate miR-137 promoter, and results in increased expression of miR-137. This is confirmed by increased levels of miR-137 at fifth day of neuronal differentiation (Figure S3B). Our result (Figure S3B) is concordant with previous studies where the expression of miR-137 was significantly upregulated when ESCs²⁴ and NSCs^{22,58} were differentiated into neuronal lineage.⁶²

However, it is surprising that OCT4, a bonafide pluripotency transcription factor, is being seen as a key player in cellular differentiation. OCT4 expression is reported in NSCs during brain development and decreases rapidly as embryo matures.⁶³ Elevated SOX2 and OCT4 levels modestly increase neuroectodermal commitment of ES cells upon differentiation.^{64,65} These observations suggest that OCT4 expression at a specific magnitude is required for inducing pluripotency, else it may favor differentiation. Binding of MECP2 and SOX2 in the enhancer region of miR-137 (2.5 kb upstream of TSS) is required for proper regulation of miR-137 in mouse adult NSCs.⁵⁸ Therefore, we speculate that miR-137 induces the expression of SIRT1 which in turn upregulates miR-137 expression by increasing OCT4 and SOX2 levels and this forms a feed-forward self-regulatory loop (Figure 7E). However, our speculation merits further validation.

Our study demonstrated that MEF2A is a direct target of miR-137 (Figure 3). miR-137-mediated downregulation of MEF2A, which is an upstream transcriptional regulator of PGC1 α ,⁶⁶ might cause impaired transcription of PGC1 α (Figures 4A,B and 7E). Notably, PGC1 α is also a predicted target of miR-137.^{43,44} The binding site of miR-137 in the 3'UTR of PGC1 α is evolutionarily conserved across various mammalian species (Figure S4A,B). Modulation of PGC1 α levels by miR-137 (Figure 4A,B; Figure S4C) suggested that miR-137 downregulates PGC1 α . However, further experiments are warranted to conclude that PGC1 α is a target of miR-137. Upregulation of NRF2 and TFAM by miR-137 indicates that mitochondrial biogenesis is induced in hiNSCs even in the presence of low levels of PGC1 α . These results are in harmony with previous studies which demonstrate induction of mitochondrial biogenesis in the absence of PGC1 α .^{61,62}

MiR-137-mediated increased expression of NRF2⁶⁷ might be due to increased levels of SIRT1 and AMPK^{49,52} (Figure 4A,B). NRF2, in turn, induced expression of TFAM by transcriptional activation (Figure 7E).⁶⁸ TFAM can also be induced by mTORC1 which was also found to be elevated by miR-137 (Figure 4A).⁶⁹ Subsequently, TFAM-enhanced mitochondrial DNA replication and biogenesis as shown by increase in mtDNA copy number and mitochondria content. This is followed by the activation of OXPHOS machinery and OCR

(Figure 6B-D). miR-137 represses hypoxia-induced mitophagy,⁷⁰ therefore, it might shut down mitochondria degradation pathway to promote mitochondria biogenesis. Our findings support that miR-137 is a new small noncoding RNA regulating the energy homeostasis pathway during neural development.

Mitochondrial dynamics is defined by a delicate balance between fusion and fission processes and these processes promote commitment of NSCs to neuronal differentiation.^{29,30,71,72} In our study, miR-137 modulates mitochondrial fusion and fission (Figure 5), which result in morphological changes in mitochondria. These morphological adaptations are necessary for metabolic shift of cells from glycolysis to OXPHOS. Therefore, miR-137 regulates mitochondrial dynamics to attain neuronal fate of hiNSCs.

We have delineated molecular circuitry associated with the development of human neurons using hiPSC-derived NSCs as an in vitro model system. Our study shows that miR-137 promotes mitochondrial fusion and fission, and increases mitochondrial biogenesis and OXPHOS to match the need of newly formed neurons.

6 | CONCLUSION

Neurogenesis decreases throughout the life span of an adult and results in compromised regenerative and repair capacity of the brain.⁷³ Therefore, novel molecules/strategies responsible for enhancing NSC commitment and differentiation, especially for aging-associated neurodegenerative diseases, are needs of the hour. Thus, miR-137-based intervention might be useful for the management of aging-associated neurodegenerative diseases in future.

ACKNOWLEDGMENTS

This research was supported by DST INSPIRE Faculty grant (Code-IFA 13-LSBM-90). INSPIRE Faculty fellowship to Y.K.A. by the Department of Science and Technology (DST), India is greatly acknowledged. The funding agency had no role in the writing of manuscript or in the decision to submit the article for publication. We also acknowledge National Brain Research Centre (NBRC) core funds, Manesar, India, to both P.S. and Y.K.A. Resource help from Anurag Agrawal, Director, CSIR-IGIB and Anirban Basu, NBRC is greatly acknowledged. We thank Reshma Bhagat, Naveen Kumar, Bhavya Gohil, and Naushad Alam for technical assistance and Priyanka Ghosh for manuscript editing. We are grateful to Anand Swaroop, NEI, NIH (Bethesda, MD) for insightful comments and for improving the narrative of manuscript. We are thankful to Dr. Vijender Chaitankar, NHLBI, NIH (Bethesda) for manuscript editing. We acknowledge support from Distributed Information Centre at NBRC. We thank Neeraj Jain, Director, NBRC for the kind support.

CONFLICT OF INTEREST

The authors declared no potential conflicts of interest.

AUTHOR CONTRIBUTIONS

A.S.C.: conception and design, collection and/or assembly of data, data analysis and interpretation, manuscript writing, and final approval

of manuscript; T.S.: collection and/or assembly of data and final approval of manuscript; B.P.: collection and/or assembly of data, data analysis and interpretation, and final approval of manuscript; K.G.: data analysis and interpretation, and final approval of manuscript; P.S.: administrative support, provision of study material or subjects, and final approval of manuscript; Y.K.A.: conception and design, collection and/or assembly of data, data analysis and interpretation, manuscript writing, and final approval of manuscript.

DATA AVAILABILITY STATEMENT

The data that support the findings of this study are available from the corresponding author upon reasonable request.

ORCID

Pankaj Seth  <https://orcid.org/0000-0003-1021-7839>

Yogita K. Adlakha  <https://orcid.org/0000-0002-0922-1921>

REFERENCES

- Stiles J, Jernigan TL. The basics of brain development. *Neuropsychol Rev*. 2010;20(4):327-348.
- Pilaz LJ, Silver DL. Post-transcriptional regulation in corticogenesis: how RNA-binding proteins help build the brain. *Wiley Interdiscip Rev RNA*. 2015;6(5):501-515.
- Rice D, Barone SJ. Critical periods of vulnerability for the developing nervous system: evidence from humans and animal models. *Environ Health Perspect*. 2000;108(Suppl 3):511-533.
- Sun E, Shi Y. MicroRNAs: small molecules with big roles in neurodevelopment and diseases. *Exp Neurol*. 2015;268:46-53.
- Lai EC. Micro RNAs are complementary to 3' UTR sequence motifs that mediate negative post-transcriptional regulation. *Nat Genet*. 2002;30(4):363-364.
- Bushati N, Cohen SM. microRNA functions. *Annu Rev Cell Dev Biol*. 2007;23:175-205.
- Hwang HW, Mendell JT. MicroRNAs in cell proliferation, cell death, and tumorigenesis. *Br J Cancer*. 2006;94(6):776-780.
- Karp X, Ambros V. Developmental biology. Encountering microRNAs in cell fate signaling. *Science*. 2005;310(5752):1288-1289.
- Fiore R, Siegel G, Schratz G. MicroRNA function in neuronal development, plasticity and disease. *Biochim Biophys Acta*. 2008;1779(8):471-478.
- Boyer LA, Lee TI, Cole MF, et al. Core transcriptional regulatory circuitry in human embryonic stem cells. *Cell*. 2005;122(6):947-956.
- Willemsen MH, Valles A, Kirkels LA, et al. Chromosome 1p21.3 microdeletions comprising DPYD and MIR137 are associated with intellectual disability. *J Med Genet*. 2011;48(12):810-818.
- Strazisar M, Cammaerts S, van der Ven K, et al. MIR137 variants identified in psychiatric patients affect synaptogenesis and neuronal transmission gene sets. *Mol Psychiatry*. 2015;20(4):472-481.
- Consortium. SPG-WASG. Genome-wide association study identifies five new schizophrenia loci. *Nat Genet*. 2011;43(10):969-976.
- Whalley HC, Papmeyer M, Romaniuk L, et al. Impact of a microRNA MIR137 susceptibility variant on brain function in people at high genetic risk of schizophrenia or bipolar disorder. *Neuropsychopharmacology*. 2012;37(12):2720-2729.
- Soldati C, Bithell A, Johnston C, Wong KY, Stanton LW, Buckley NJ. Dysregulation of REST-regulated coding and non-coding RNAs in a cellular model of Huntington's disease. *J Neurochem*. 2013;124(3):418-430.
- Wu H, Tao J, Chen PJ, et al. Genome-wide analysis reveals methyl-CpG-binding protein 2-dependent regulation of microRNAs in a mouse model of Rett syndrome. *Proc Natl Acad Sci USA*. 2010;107(42):18161-18166.

17. Devanna P, Vernes SC. A direct molecular link between the autism candidate gene RORa and the schizophrenia candidate MIR137. *Sci Rep*. 2014;4:3994.
18. Silber J, Lim DA, Petritsch C, et al. miR-124 and miR-137 inhibit proliferation of glioblastoma multiforme cells and induce differentiation of brain tumor stem cells. *BMC Med*. 2008;6:14.
19. Althoff K, Beckers A, Odersky A, et al. MiR-137 functions as a tumor suppressor in neuroblastoma by downregulating KDM1A. *Int J Cancer*. 2013;133(5):1064-1073.
20. Balaguer F, Link A, Lozano JJ, et al. Epigenetic silencing of miR-137 is an early event in colorectal carcinogenesis. *Cancer Res*. 2010;70(16):6609-6618.
21. Adlakha YK, Saini N. Brain microRNAs and insights into biological functions and therapeutic potential of brain enriched miRNA-128. *Mol Cancer*. 2014;13:33.
22. Sun G, Ye P, Murai K, et al. miR-137 forms a regulatory loop with nuclear receptor TLX and LSD1 in neural stem cells. *Nat Commun*. 2011;2:529.
23. Tarantino C, Paoletta G, Cozzuto L, et al. miRNA 34a, 100, and 137 modulate differentiation of mouse embryonic stem cells. *FASEB J*. 2010;24(9):3255-3263.
24. Jiang K, Ren C, Nair VD. MicroRNA-137 represses Klf4 and Tbx3 during differentiation of mouse embryonic stem cells. *Stem Cell Res*. 2013;11(3):1299-1313.
25. Agostini M, Annicchiarico-Petruzzelli M, Melino G, Rufini A. Metabolic pathways regulated by TAp73 in response to oxidative stress. *Oncotarget*. 2016;7(21):29881-29900.
26. Beckervordersandforth R, Ebert B, Schaffner I, et al. Role of mitochondrial metabolism in the control of early lineage progression and aging phenotypes in adult hippocampal neurogenesis. *Neuron*. 2017;93(3):560-573.e566.
27. Khacho M, Clark A, Svoboda DS, et al. Mitochondrial dynamics impacts stem cell identity and fate decisions by regulating a nuclear transcriptional program. *Cell Stem Cell*. 2016;19(2):232-247.
28. Chen CT, Shih YR, Kuo TK, et al. Coordinated changes of mitochondrial biogenesis and antioxidant enzymes during osteogenic differentiation of human mesenchymal stem cells. *STEM CELLS*. 2008;26(4):960-968.
29. Steib K, Schaffner I, Jagasia R, Ebert B, Lie DC. Mitochondria modify exercise-induced development of stem cell-derived neurons in the adult brain. *J Neurosci*. 2014;34(19):6624-6633.
30. Khacho M, Slack RS. Mitochondrial dynamics in the regulation of neurogenesis: from development to the adult brain. *Dev Dyn*. 2018;247(1):47-53.
31. Beers J, Linask KL, Chen JA, et al. A cost-effective and efficient reprogramming platform for large-scale production of integration-free human induced pluripotent stem cells in chemically defined culture. *Sci Rep*. 2015;5:11319.
32. Beers J, Gulbranson DR, George N, et al. Passaging and colony expansion of human pluripotent stem cells by enzyme-free dissociation in chemically defined culture conditions. *Nat Protoc*. 2012;7(11):2029-2040.
33. Mishra M, Taneja M, Malik S, Khalique H, Seth P. Human immunodeficiency virus type 1 tat modulates proliferation and differentiation of human neural precursor cells: implication in NeuroAIDS. *J Neurovirol*. 2010;16(5):355-367.
34. Jacques TS, Relvas JB, Nishimura S, et al. Neural precursor cell chain migration and division are regulated through different beta1 integrins. *Development*. 1998;125(16):3167-3177.
35. Bhagat R, Prajapati B, Narwal S, et al. Zika virus E protein alters the properties of human fetal neural stem cells by modulating microRNA circuitry. *Cell Death Differ*. 2018;25(10):1837-1854.
36. Pfaffl MW. A new mathematical model for relative quantification in real-time RT-PCR. *Nucleic Acids Res*. 2001;29(9):e45.
37. Adlakha YK, Saini N. miR-128 exerts pro-apoptotic effect in a p53 transcription-dependent and -independent manner via PUMA-Bak axis. *Cell Death Dis*. 2013;4:e542.
38. Quiros PM, Goyal A, Jha P, Auwerx J. Analysis of mtDNA/nDNA ratio in mice. *Curr Protoc Mouse Biol*. 2017;7(1):47-54.
39. Adlakha YK, Saini N. MicroRNA-128 downregulates Bax and induces apoptosis in human embryonic kidney cells. *Cell Mol Life Sci*. 2011;68(8):1415-1428.
40. Kee N, Sivalingam S, Boonstra R, Wojtowicz JM. The utility of Ki-67 and BrdU as proliferative markers of adult neurogenesis. *J Neurosci Methods*. 2002;115(1):97-105.
41. Blockus H, Chedotal A. Slit-Robo signaling. *Development*. 2016;143(17):3037-3044.
42. Buchsbaum IY, Cappello S. Neuronal migration in the CNS during development and disease: insights from in vivo and in vitro models. *Development*. 2019;146(1):dev163766.
43. Agarwal V, Bell GW, Nam JW, Bartel DP. Predicting effective microRNA target sites in mammalian mRNAs. *Elife*. 2015;4:4. <https://doi.org/10.7554/eLife.05005>.
44. Paraskevopoulou MD, Georgakilas G, Kostoulas N, et al. DIANA-microT web server v5.0: service integration into miRNA functional analysis workflows. *Nucleic Acids Res*. 2013;41:W169-W173.
45. Xiao J, Peng F, Yu C, et al. microRNA-137 modulates pancreatic cancer cells tumor growth, invasion and sensitivity to chemotherapy. *Int J Clin Exp Pathol*. 2014;7(11):7442-7450.
46. Fernandez-Marcos PJ, Auwerx J. Regulation of PGC-1alpha, a nodal regulator of mitochondrial biogenesis. *Am J Clin Nutr*. 2011;93(4):884S-890S.
47. Wu Z, Puigserver P, Andersson U, et al. Mechanisms controlling mitochondrial biogenesis and respiration through the thermogenic coactivator PGC-1. *Cell*. 1999;98(1):115-124.
48. Wilkins HM, Harris JL, Carl SM, et al. Oxaloacetate activates brain mitochondrial biogenesis, enhances the insulin pathway, reduces inflammation and stimulates neurogenesis. *Hum Mol Genet*. 2014;23(24):6528-6541.
49. Chai D, Zhang L, Xi S, Cheng YY, Jiang H, Hu R. Nrf2 activation induced by Sirt1 ameliorates acute lung injury after intestinal ischemia/reperfusion through NOX4-mediated gene regulation. *Cell Physiol Biochem*. 2018;46(2):781-792.
50. Chapman NM, Zeng H, Nguyen TM, et al. mTOR coordinates transcriptional programs and mitochondrial metabolism of activated Treg subsets to protect tissue homeostasis. *Nat Commun*. 2018;9(1):2095.
51. Liu XM, Peyton KJ, Shebib AR, et al. Activation of AMPK stimulates heme oxygenase-1 gene expression and human endothelial cell survival. *Am J Physiol*. 2011;300(1):H84-H93.
52. Joo MS, Kim WD, Lee KY, Kim JH, Koo JH, Kim SG. AMPK facilitates nuclear accumulation of Nrf2 by phosphorylating at serine 550. *Mol Cell Biol*. 2016;36(14):1931-1942.
53. Peng K, Yang L, Wang J, et al. The interaction of mitochondrial biogenesis and fission/fusion mediated by PGC-1alpha regulates rotenone-induced dopaminergic neurotoxicity. *Mol Neurobiol*. 2017;54(5):3783-3797.
54. Panopoulos AD, Yanes O, Ruiz S, et al. The metabolome of induced pluripotent stem cells reveals metabolic changes occurring in somatic cell reprogramming. *Cell Res*. 2012;22(1):168-177.
55. Varum S, Rodrigues AS, Moura MB, et al. Energy metabolism in human pluripotent stem cells and their differentiated counterparts. *PLoS One*. 2011;6(6):e20914.
56. Gogel S, Gubernator M, Minger SL. Progress and prospects: stem cells and neurological diseases. *Gene Ther*. 2010;18(1):1-6.
57. Zahr SK, Kaplan DR, Miller FD. Translating neural stem cells to neurons in the mammalian brain. *Cell Death Differ*. 2019;26(12):2495-2512.
58. Szulwach KE, Li X, Smrt RD, et al. Cross talk between microRNA and epigenetic regulation in adult neurogenesis. *J Cell Biol*. 2010;189(1):127-141.
59. Smrt RD, Szulwach KE, Pfeiffer RL, et al. MicroRNA miR-137 regulates neuronal maturation by targeting ubiquitin ligase mind bomb-1. *STEM CELLS*. 2010;28(6):1060-1070.

60. Liu L, Liu C, Zhang Q, et al. SIRT1-mediated transcriptional regulation of SOX2 is important for self-renewal of liver cancer stem cells. *Hepatology*. 2016;64(3):814-827.
61. Williams EO, Taylor AK, Bell EL, Lim R, Kim DM, Guarente L. Sirtuin 1 promotes deacetylation of Oct4 and maintenance of naive pluripotency. *Cell Rep*. 2016;17(3):809-820.
62. Shin KK, Kim YS, Kim JY, Bae YC, Jung JS. miR-137 controls proliferation and differentiation of human adipose tissue stromal cells. *Cell Physiol Biochem*. 2014;33(3):758-768.
63. Lee SH, Jeyapalan JN, Appleby V, Mohamed Noor DA, Sottile V, Scotting PJ. Dynamic methylation and expression of Oct4 in early neural stem cells. *J Anat*. 2010;217(3):203-213.
64. Strebinger D, Deluz C, Friman ET, et al. Endogenous fluctuations of OCT4 and SOX2 bias pluripotent cell fate decisions. *Mol Syst Biol*. 2019;15(9):e9002.
65. Shimozaki K, Nakashima K, Niwa H, et al. Involvement of Oct3/4 in the enhancement of neuronal differentiation of ES cells in neurogenesis-inducing cultures. *Development*. 2003;130(11):2505-2512.
66. Ramachandran B, Yu G, Gulick T. Nuclear respiratory factor 1 controls myocyte enhancer factor 2A transcription to provide a mechanism for coordinate expression of respiratory chain subunits. *J Biol Chem*. 2008;283(18):11935-11946.
67. Dinkova-Kostova AT, Abramov AY. The emerging role of Nrf2 in mitochondrial function. *Free Radic Biol Med*. 2015;88(Pt B):179-188.
68. Wu KLH, Wu CW, Chao YM, Hung CY, Chan JYH. Impaired Nrf2 regulation of mitochondrial biogenesis in rostral ventrolateral medulla on hypertension induced by systemic inflammation. *Free Radic Biol Med*. 2016;97:58-74.
69. Morita M, Gravel SP, Hulea L, et al. mTOR coordinates protein synthesis, mitochondrial activity and proliferation. *Cell Cycle*. 2015;14(4):473-480.
70. Li W, Zhang X, Zhuang H, et al. MicroRNA-137 is a novel hypoxia-responsive microRNA that inhibits mitophagy via regulation of two mitophagy receptors FUNDC1 and NIX. *J Biol Chem*. 2014;289(15):10691-10701.
71. Fang D, Yan S, Yu Q, Chen D, Yan SSD. Mfn2 is required for mitochondrial development and synapse formation in human induced pluripotent stem cells/hiPSC derived cortical neurons. *Sci Rep*. 2016;6:31462.
72. Adlakha YK, Seth P. The expanding horizon of MicroRNAs in cellular reprogramming. *Prog Neurobiol*. 2017;148:21-39.
73. Lledo PM, Alonso M, Grubb MS. Adult neurogenesis and functional plasticity in neuronal circuits. *Nat Rev Neurosci*. 2006;7(3):179-193.

SUPPORTING INFORMATION

Additional supporting information may be found online in the Supporting Information section at the end of this article.

How to cite this article: Channakkar AS, Singh T, Pattnaik B, Gupta K, Seth P, Adlakha YK. MiRNA-137-mediated modulation of mitochondrial dynamics regulates human neural stem cell fate. *Stem Cells*. 2020;38:683–697. <https://doi.org/10.1002/stem.3155>